THE JOURNAL OF PHYSICAL CHEMISTRY C

Article

pubs.acs.org/JPCC

# Mechanism of Nonlinear Optical Enhancement and Supramolecular Isomerism in 1D Polymeric Zn(II) and Cd(II) Sulfates with Pyridine-4-aldoxime Ligands

Lilia Croitor,[†] Eduard B. Coropceanu,[‡] Artëm E. Masunov,*[,§,∥] Hector J. Rivera-Jacquez,[§] Anatolii V. Siminel,[†] and Marina S. Fonari*[,†]

[†]Institute of Applied Physics, Academy of Sciences of Moldova, Academy str., 5, MD2028 Chisinau, R. Moldova

[‡]Institute of Chemistry, Academy of Sciences of Moldova, Academy str., 3, MD2028, Chisinau, R. Moldova

[§]NanoScience Technology Center, and Department of Chemistry, University of Central Florida, Orlando, Florida 32826, United States

[∥]Department of Physics, and Florida Solar Energy Center, University of Central Florida, Orlando, Florida 32826, United States

Supporting Information

**ABSTRACT:** Interaction of zinc(II) and cadmium(II) sulfates with pyridine-4-aldoxime (4-pyao) and pyridine-4-amidoxime (4-pyamo) ligands resulted in four 1D metal−organic materials (MOMs) with identical composition, $[M(SO_4)A_2(H_2O)_2]_n$, where M = Zn(II), A = 4-pyao for **1**, M = Cd(II), A = 4-pyao for **2**, M = Zn(II), A = 4-pyamo for **3**, M = Cd(II), A = 4-pyamo for **4**, and mononuclear $[Zn(SO_4)(4\text{-pyamo})_2(H_2O)_3]$ **5**. New coordination polymers represent the mixed-ligand supramolecular isomers different by the twisting of two pyridine-4-oxime ligands in the metal coordination environments, and crystallizing in the different space groups. Conformational preferences and nonlinear optical properties of the 4-pyao and 4-pyamo complexes were investigated using density functional theory. Spectral properties of **1**−**3** have been also evaluated. The solid-state emission of 1D polymers **1**−**3** appears to be ligand-based, as the positions of the emission maxima remain practically unchanged from free ligand to complexes. The enhancement of luminescence and two-photon absorption in polymers in comparison with the pure ligands is attributed to the chelation of the ligand to the metal center. The detailed mechanism of this enhancement upon complex formation is analyzed and can be used in future design of metal−organic nonlinear optical materials.

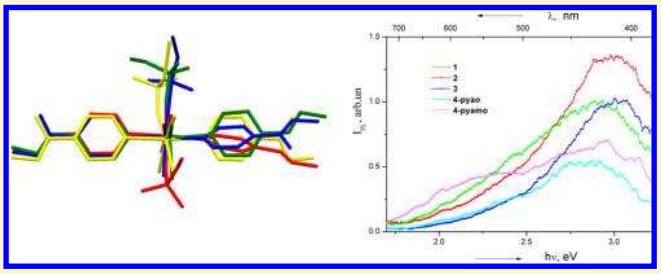


## INTRODUCTION

The rational selection of metal centers and organic ligands with suitable shape, functionality, flexibility, and symmetry plays a key role in producing metal−organic materials (MOMs) with desired structures and properties.[1−7] The versatile coordination abilities of Zn(II) and Cd(II) allow a wide variety of architectures resulting from the self-assembly of these metals with organic ligands.[8−13] Organic bridging ligands, which contain adjustable flexibility and connectivity information, play crucial role in construction and structural variations of coordination polymers (CP).[14−16] The phenomenon of supramolecular isomerism (SI) in MOMs was first generalized by Moulton and Zaworotko in 2001.[17] For the past decade it has been disclosed in and enriched by a series of low- and high-dimensional MOMs. Although the origin of this phenomenon is not completely understood, and the generation of supramolecular isomers occurs primarily serendipitously, the interest to this event continues to grow, and some reports declare the preparation of supramolecular isomers by design.[18−22] Recent examples demonstrate SI in individual Zn(II) and Cd(II) series,[23−27] and although it was suggested that the similar in electronic $d^{10}$ configuration but different in the radii Zn(II) and Cd(II) ions contribute to forming different coordination networks,[8−13] these metals are also capable to produce from the same starting materials alongside the isomorphous crystal structures the supramolecular isomers distinguished either by the conformation of the bridging ligands or by the crystal packing of the identical coordination arrays.[28−30]

Nonlinear optical (NLO) properties of MOMs are being investigated in relation to several technological applications, including optical communications and upconversion lazing.[31] Third order nonlinearities, such as two-photon absorption (2PA) present special interest, as they are not limited to non-centrosymmetric structures, unlike second harmonic generation and other second-order nonlinear optical properties. Several studies indicated[32,33] that 2PA properties are enhanced by metal coordination in MOMs, when compared to free ligands. The

**Received:** January 21, 2014
**Revised:** March 26, 2014
**Published:** April 18, 2014

mechanism of this enhancement is not well understood. Supramolecular isomerism provides an excellent opportunity to investigate the role of ligand organization in the coordination sphere on 2PA materials design. Ligand assembly in MOM is more robust and well defined than noncovalent aggregation of the chromophores, which was shown (both in crystalline phase[35] and in aqueous solution[36]) to result in the coupling of the excited states of the monomers. In a dimer, this coupling produces symmetric and antisymmetric combinations, shifted up and down in energy with respect to the monomeric states. Since selection rules for 1PA and 2PA absorption differ, the blue shift on the linear absorption spectra is accompanied by the red shift on 2PA spectrum and vice versa. These findings were recently reported by some of us[35,36] and independently confirmed.[37] Having been targeted at the hybrid polymeric materials with cumulative properties (luminescence and guest inclusion in our case), we have demonstrated the efficacy of the oxime/anion/aromatic amine "blend" approach[38,39] and succeeded in preparation of Zn(II) and Cd(II) mixed-ligand MOMs of different dimensionalities where the bulky classic dioximes or pyridine-*n*-aldoxime ($n$ = 2 for 2-pyao, $n$ = 4 for 4-pyao) molecules act as auxiliary ligands whose coordination to the metal centers provides the loosely packed materials with the voids occupied (or might be potentially occupied) by small organic molecules.[28−30,34,40−43] The very limited crystallographic data available for MOMs with pyridine-4-oxime ligands (Scheme 1) reveals the monodentate mode of 4-pyao coordination to the metal center via pyridine nitrogen.[42,45−53]

**Scheme 1. Ligands Used in This Study: (a) Pyridine-4-aldoxime (4-pyao); (b) Pyridine-4-amidoxime (4-pyamo)**

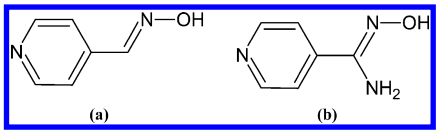


The very recent study documented the 4-pyamo bridging function that is coordinated to the Ag(I) and Cu(I) metal centers via both pyridine and oxime nitrogens, giving rise to the one-dimensional 1D and 2D coordination polymers.[54] The sulfate anion, as a simple tetrahedral oxo-anion, has versatile coordination modes including monodentate, bidentate bridging, bidentate chelating, tridentate bridging, and even tetradentate bridging, thus providing extensions of structures.[44] We have recently demonstrated that the combination of Zn(II) or Cd(II) sulfates with 2-pyao resulted in a series of MOMs through the successive substitution of water molecules by sulfate bridges in the metal coordination environments.[43] From the crystal engineering viewpoint, this gave rise to the hybrid solids of different dimensionalities, including mono-, binuclear, and 1D polymeric materials, whose interest for the materials science and primarily for NLO applications might arise from the acentricity of the synthetized 1D polymeric materials, $[Zn(SO_4)(2\text{-pya})(H_2O)_2]_n$ and $[Cd(SO_4)(2\text{-pya})(H_2O)]_n$, with the less amount of water in favor of sulfate anions in the metal coordination cores. Keeping that in mind, we have performed the reactions of zinc and cadmium sulfates with 4-pyao and 4-pyamo ligands (Scheme 1) and produced five new MOMs including four 1D CPs with similar compositions, $[Zn(SO_4)(4\text{-pyao})_2(H_2O)_2]_n$ **1**, $[Cd(SO_4)(4\text{-pyao})_2(H_2O)_2]_n$ **2**, $[Zn(SO_4)(4\text{-pyamo})_2(H_2O)_2]_n$ **3**, and $[Cd(SO_4)(4\text{-pyamo})_2(H_2O)_2]_n$ **4**, and mononuclear $[Zn(SO_4)(4\text{-pyamo})_2(H_2O)_3]$ **5**. Herein we present the structures, luminescence, and predicted NLO properties for these new crystalline solids.

## EXPERIMENTAL AND COMPUTATIONAL DETAILS

**Starting Materials and General procedures.** Full synthetic and characterization details are provided in the Supporting Information. All starting materials and solvents were used without further purification.

**X-ray Diffraction Studies.** Diffraction measurements for **1**−**5** were carried out at room temperature on a Xcalibur "Oxford Diffraction" diffractometer equipped with CCD area detector and a graphite monochromator utilizing MoK$\alpha$ radiation at room temperature. Final unit cell dimensions were obtained and refined on an entire data set. Lorentz and polarization corrections were applied for diffracted reflections. In addition, the data were corrected for empirical absorption using spherical harmonics, implemented in SCALE3 ABSPACK scaling algorithm. All calculations to solve the structures and to refine the models were carried out with the programs SHELXS97 and SHELXL97.[55] The C-bound H-atoms were placed in calculated positions and were treated using a riding model approximation with $U_{iso}(H) = 1.2U_{eq}(C)$, while the O-bound H-atoms were found from differential Fourier maps at intermediate stages of the refinement and their positions were constrained using the AFIX 83 instruction in SHELXL for oxime groups and DFIX instruction for water molecules. These hydrogen atoms were refined with isotropic displacement parameter $U_{iso}(H) = 1.5U_{eq}(O)$. Figures 1 and 2 were produced using MERCURY.[56]

**Computational Methods.** In order to rationalize the conformational differences between Zn and Cd complexes in position of the oxime ligands, the density functional theory calculations were performed using Gaussian 09.[57] We studied the monomer complex units for compounds **1**−**5** using the polarizable continuum model with dielectric constant of 2 in order to simulate the crystalline environment, and M05-QX exchange-correlation functional (formerly known as M05-11/4X),[58] obtained by interpolation between M05 and M05-2X functionals[59] and including 35% of the exact exchange. We used SDD Stuttgart effective core potentials for the metal atoms[60] and D95 basis set for the other atoms.[61]

Prediction of the linear absorption spectra using linear response time dependent density functional theory[62] (TD-DFT) nowadays is routine.[63−65] Optimization and the minimum energy passway search on the excited state potential surface made it possible recently to predict emission[66,67] (including dual emission[43,68,69]) and photochemical reaction[70−74] processes. In order to predict 2PA cross section profiles, we employed a posteriori Tamm-Dancoff approximation[75] (ATDA) to second order coupled electronic oscillator formalism,[76,77] applied at the TD-DFT[78] level. In this approximation, the excitation energies $\omega_{0X}$ and transition densities $\xi_X$ between the ground and excited states are obtained as solutions to the habitual linear response TD-DFT equations. Therefore, transition dipoles are calculated as a convolution of the dipole moment operator $\mu$ with respective transition densities

$$\mu_{0X} = \langle 0|\mu|X\rangle = Tr(\mu\xi_X) \quad (1)$$

Here, the ground state is denoted by $|0\rangle$, whereas 1PA and 2PA excited states are labeled by $|X\rangle$ and $|Y\rangle$, respectively. At the same time, Tamm-Dancoff formulas are used to predict state-to-state transition dipoles $\mu_{XY}$ and differences between the permanent and ground state dipole moments ($\mu_{XX} = \mu_X - \mu_0$) as


dx.doi.org/10.1021/jp5007395 | J. Phys. Chem. C 2014, 118, 9217−9227

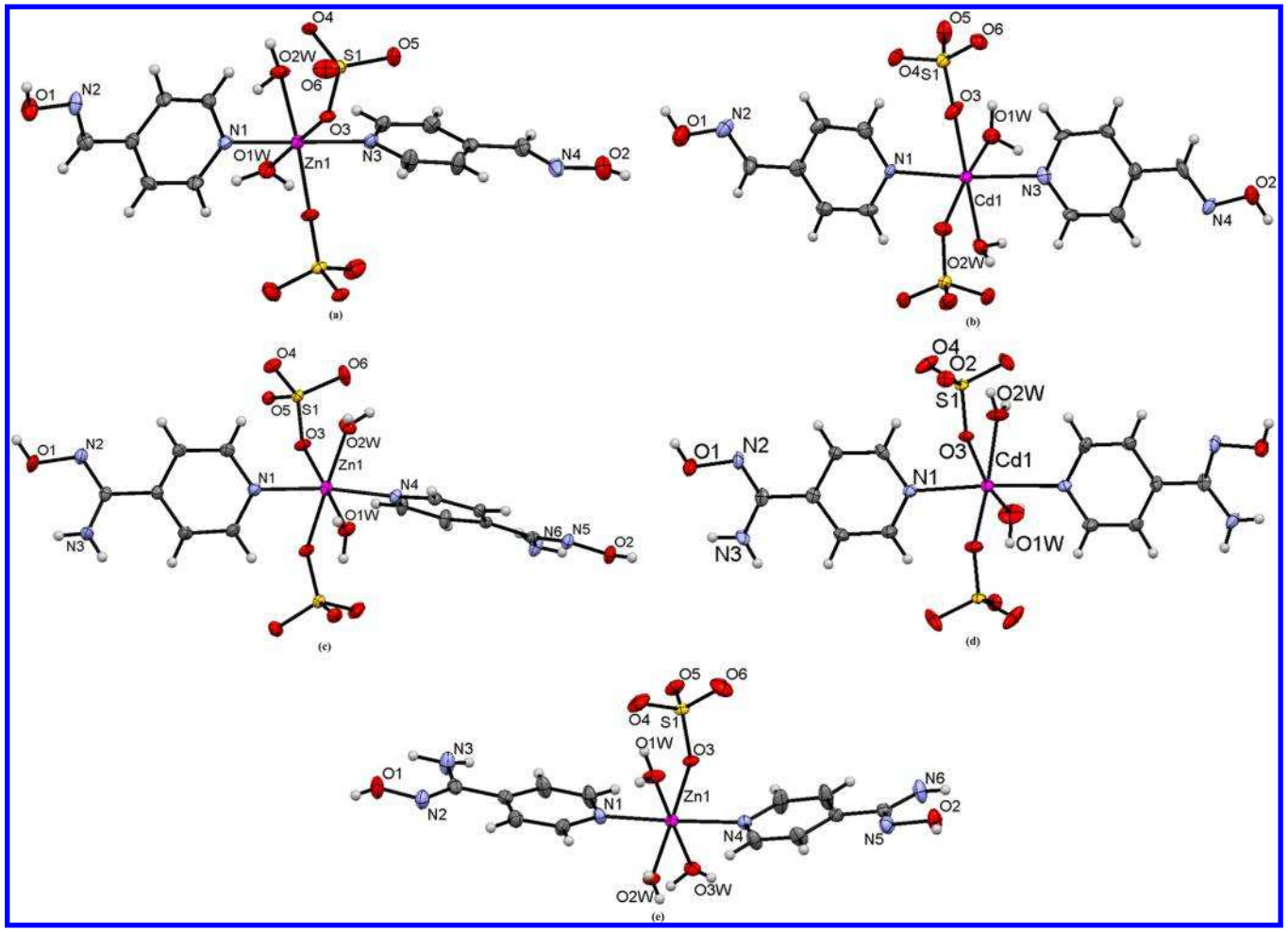


**Figure 1.** Coordination surroundings of metal ions in **1**−**5** with the partial atom labeling: (a) **1**, (b) **2**, (c) **3**, (d) **4**, and (e) **5**.

$$\mu_{XY} = \langle X|\mu|Y\rangle = Tr(\mu(I - 2\rho)\xi_X^*\xi_Y) \quad (2)$$

$$\mu_{XX} = \langle X|\mu|X\rangle = Tr(\mu(I - 2\rho)\xi_X^*\xi_X) \quad (3)$$

since they are not available in linear response TD-DFT. Here, $I$ is the identity matrix and $\rho$ is the ground state density matrix. Both permanent[79] and state-to-state transition dipoles[75] calculated this way were validated previously by comparison with the high theory level coupled cluster results. These values are then used in the Sum over States (SOS) expression[80] to predict the two-photon transition matrix elements

$$M_{\alpha\beta}^{Y} = \frac{1}{2\hbar}\sum_{X}\left(\frac{\langle Y|\mu_\alpha|X\rangle\langle X|\mu_\beta|0\rangle}{\left(\omega_{0X} - \frac{\omega_{0Y}}{2}\right) - i\Gamma_{X0}} + \frac{\langle Y|\mu_\beta|X\rangle\langle X|\mu_\alpha|0\rangle}{\left(\omega_{0X} - \frac{\omega_{0Y}}{2}\right) - i\Gamma_{X0}}\right) \quad (4)$$

where $\alpha$ and $\beta$ run over $x$, $y$, and $z$ spatial directions. The factor $(\omega_{0X} - \omega_{0Y}/2)$ is called the detuning between the 1PA state and the virtual state (midway in energy between the ground and the 2PA state), and $\Gamma_{X0}$ is the damping constant. The orientationally averaged 2PA cross section for linearly polarized beam is then computed by substituting the transition matrix components (eq 4) into the formula

$$\sigma^{(2)}(\omega) = \frac{16\pi^3\omega^2}{15c^2n^2}\sum_{Y}\sum_{x,y,z}^{\beta}\sum_{x,y,z}^{\alpha}(M_{\alpha\alpha}^{Y}M_{\beta\beta}^{Y}{}^* + 2M_{\alpha\beta}^{Y}M_{\alpha\beta}^{Y}{}^*)\, g_Y(2\omega) \quad (5)$$

Here $\omega = \omega_{0Y}/2$ and $g_Y(2\omega)$ is the Lorentzian line shape function given by

$$g_Y(2\omega) = \frac{1}{\pi}\frac{\Gamma_{Y0}}{(\omega_{Y0} - 2\omega)^2 + \Gamma_{Y0}{}^2} \quad (6)$$

The line width $\Gamma_{Y0}$ accounts for the experimentally observed homogeneous and inhomogeneous broadening and is usually taken as an empirical constant (0.1 eV in our calculations). The specific choice of the damping constant $\Gamma_{X0}$ and the Lorentzian line shape function was suggested in both experimental[81] and computational[82] studies. The proper choice of this parameter should reproduce experimentally observed linewidths. However, even without variation of this empirical parameter, the ATDA method was benchmarked favorably in comparison with experimental 2PA profiles and predictions by other methods[83] and successfully used to predict 2PA profiles accurately for a wide range of NLO chromophores.[54,68,72,73,84−90] We implemented ATDA method in the local version of Gaussian 09 code.

## RESULTS AND DISCUSSION

The MOMs **1**−**5** were obtained in the identical synthetic conditions (see Supporting Information) by mixing the warm


dx.doi.org/10.1021/jp5007395 | J. Phys. Chem. C 2014, 118, 9217−9227

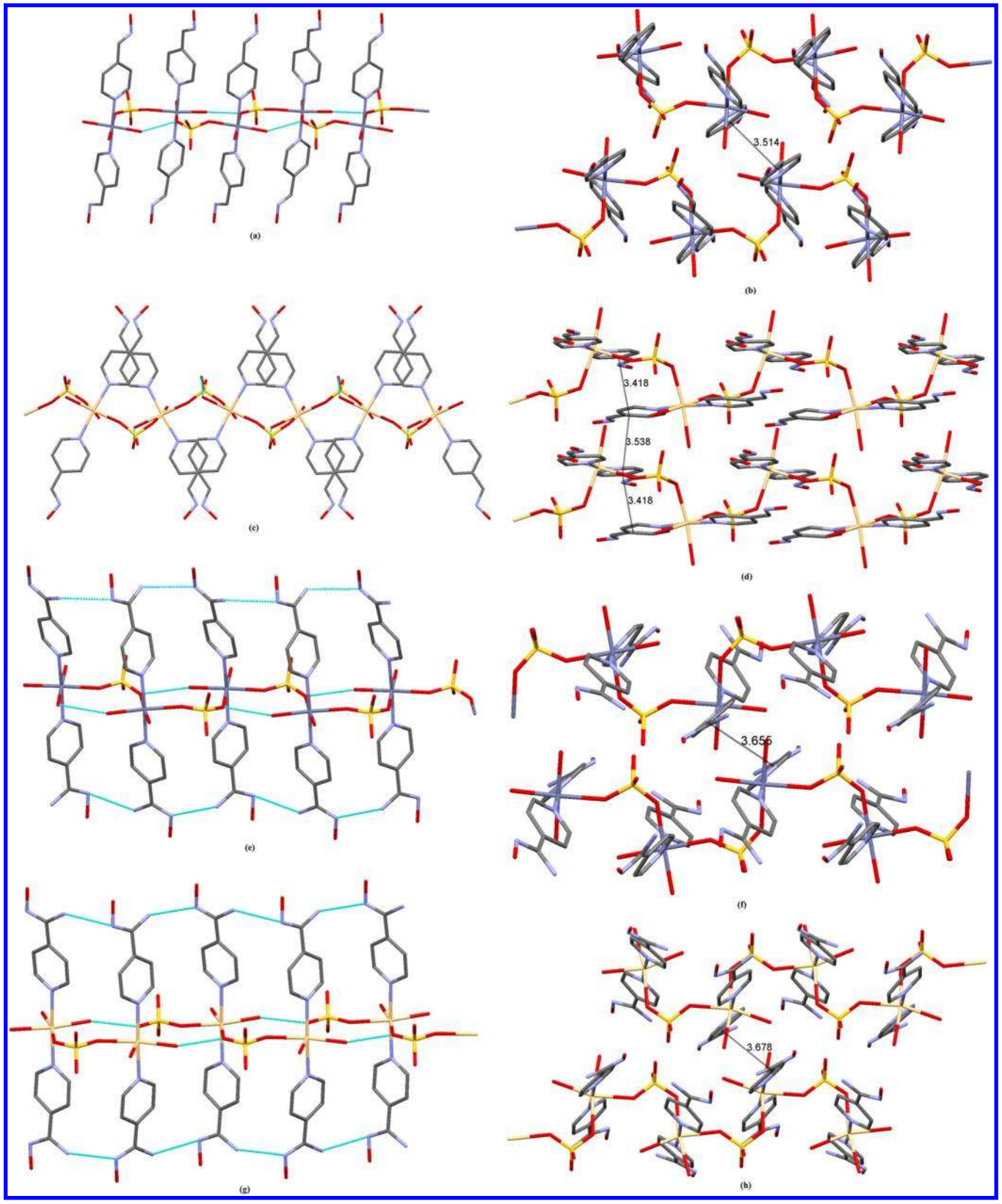


**Figure 2.** Top and side projections of polymeric chains in **1** (a, b), **2** (c, d), **3** (e, f), and **4** (g, h). The shortest separations between the overlapping aromatic moieties are indicated.

solutions of the corresponding starting sulfate salts, and the corresponding pyridine-4-aldoxime. The final crystalline solids were precipitated from the slowly cooled solutions. In the IR spectra of the complexes, the presence of sulfate anions is documented by the strong intensity bands at 1130−1057 $cm^{-1}$, while the characteristic band of coordinated water molecule is observed at ∼3377−3324 $cm^{-1}$. The presence of $NH_2$-groups in **3**−**5** is documented by the bands at 3463−3456 $cm^{-1}$. The bands


dx.doi.org/10.1021/jp5007395 | J. Phys. Chem. C 2014, 118, 9217−9227

**Table 1. Selected Crystallographic Parameters in 1−5**

| | 1 | 2 | 3 | 4 | 5 |
|---|---|---|---|---|---|
| formula | $C_{12}H_{16}N_4O_8SZn$ | $C_{12}H_{16}N_4O_8SCd$ | $C_{12}H_{18}N_6O_8SZn$ | $C_{12}H_{18}N_6O_8SCd$ | $C_{12}H_{20}N_6O_9SZn$ |
| F.W. | 441.72 | 488.75 | 471.75 | 518.78 | 489.77 |
| crystal system | orthorhombic | monoclinic | monoclinic | orthorhombic | orthorhombic |
| space group | *Pbca* | $P2_1$ | $P2_1/c$ | *Pnma* | $P2_12_12_1$ |
| *Z* | 8 | 2 | 4 | 4 | 4 |
| *a* (Å) | 9.1328(6) | 6.8863(9) | 21.2322(6) | 9.5591(10) | 7.9153(2) |
| *b* (Å) | 9.0544(5) | 10.0489(9) | 8.5552(3) | 21.864(2) | 10.9871(3) |
| *c* (Å) | 39.490(4) | 12.7212(13) | 9.4750(3) | 8.5122(8) | 21.5221(5) |
| *β* (deg) | 90.0 | 90.54(1) | 94.688(3) | 90.0 | 90.0 |
| *V* (Å) | 3265.5(4) | 880.26(17) | 1715.34(9) | 1779.1(3) | 1871.70(8) |
| $D_c$ ($Mg/m^3$) | 1.797 | 1.844 | 1.827 | 1.937 | 1.738 |
| $\mu$ ($mm^{-1}$) | 1.685 | 1.408 | 1.613 | 1.403 | 1.486 |
| *F*(000) | 1808 | 488 | 968 | 1040 | 1008 |
| data/restraints/parameters | 3021/6/247 | 2503/7/250 | 3354/12/277 | 1582/15/150 | 2890/15/293 |
| reflections collected | 6753 | 3345 | 5923 | 3609 | 4698 |
| independent reflections | 3021 [*R*(int) = 0.0394] | 2503 [*R*(int) = 0.0400] | 3354 [*R*(int) = 0.0286] | 1582 [*R*(int) = 0.0645] | 2890 [*R*(int) = 0.0223] |
| GOOF of $F^2$ | 1.103 | 1.079 | 1.023 | 1.028 | 1.062 |
| $R_1$, $wR_2$ [$I > 2\sigma(I)$] | 0.0571, 0.1038 | 0.0625, 0.1454 | 0.0366, 0.0859 | 0.0578, 0.1158 | 0.0336, 0.0723 |
| $R_1$, $wR_2$ (all data) | 0.0782, 0.1124 | 0.0678, 0.1545 | 0.0464, 0.0917 | 0.0876, 0.1293 | 0.0392, 0.0768 |

characteristic for oxime groups were registered at 1658−1640, 1239−1229, and 993−980 $cm^{-1}$. The peaks at ∼1671 and 1517−1504 $cm^{-1}$ can be attributed to the vibrations of the aromatic ring, and the band at 1427−1420 $cm^{-1}$ corresponds to the C═N stretching vibrations of the pyridine ring. Also, in all complexes, the bands at 1427−1420 $cm^{-1}$ are assigned to the $\delta$(C−H) deformation vibrations.

The main crystallographic parameters for **1**−**5** are summarized in Table 1 (the details of coordination geometry for **1**−**5** is given in the Supporting Information). The elemental analysis and single crystal X-ray investigation revealed the similar compositions for **1**−**4**, with two sulfate anions, two oxime, and two water molecules coordinated to the metal centers, that allowed considering the obtained materials as supramolecular isomers.[17] The metal coordination surroundings in **1**−**5** are shown in Figure 1. The new materials are obtained by successive substitution of water molecules coordinated to the metal center by oxime ligands and sulfate anions, as it is evident from comparison the compositions of polymeric **1**−**4** and mononuclear **5**. In all structures, the metal atoms adjust the similar $N_2O_4$ distorted octahedral coordination cores composed of two neutral oxime, and two water molecules, and two bidentate-bridging sulfate anions in **1**−**4** (Figure 1a−d), and two oxime, three water molecules, and one monodentate-coordinated sulfate anion in **5** (Figure 1e). Two oxime molecules occupy axial positions being coordinated via pyridine nitrogen, Zn−N and Cd−N distances being in the ranges 2.097(2)−2.168(4) and 2.301(7)−2.304(14) Å. The two sulfate anions and two water molecules, the similar entities being in *cis*-arrangement (Table 1S, Supporting Information), occupy the vertices in the equatorial plane, with Zn−O distances being in the range 2.110(2)−2.173(4) Å in **1**, **3**, and **5**, and Cd−O distances being in the range 2.276(13)−2.378(14) Å in **2** and **4**. The additional stabilization of the equatorial environment is provided by the OH···O hydrogen bonds between coordinated water molecules and sulfate anions (Table 2S, Supporting Information). The inspection of **1**−**4** reveals the conformational dissimilarities around the metal centers manifested in the different arrangement of two oxime molecules. The two 4-pyao molecules in **1** display in practically perpendicular planes, with the dihedral angle of 82.26° between their aromatic cores (Figure 1a), while in **2** the same angle equals to 1.60°, and the molecules display in *anti*-conformation with regard to the arrangement of oxime groups (Figure 1b). An arrangement of 4-pyamo molecules in **3**−**4** also exhibits a pronounced difference. Similar to **1**, two 4-pyamo molecules in 3 adjust the twisted arrangement described by the dihedral angle of 87.97 ° between the aromatic cores (Figure 1c), while in **4** the same angle is equal to 10.13 °, and the molecules display in *syn*-conformation with the regard to the oxime groups, the same *syn*-arrangement of 4-pyamo molecules in the mononuclear **5** is described by the dihedral angle of 17.98 ° (Figure 1d). Thus, in the studied compounds, the two coordinated oxime molecules "pass" the whole range of possible conformations, from the *syn*- to *trans*-arrangements at the metal centers.

In order to analyze the differences in conformations between Zn and Cd complexes, we performed the potential surface scan at M05-QX/SDD theory level. A model complexes **6m** and **7m** were built, where octahedral coordination around Zn (**6m**) or Cd (**7m**) was saturated by four water molecules in the equatorial plane, while two axial positions were occupied by two 4-pyao molecules. The torsion angles between the pyridine rings were fixed at values between 0.0° and 180.0°, with 10° step size. All other degrees of freedom were optimized. The resulting potential curves were found to have minima at nearly perpendicular conformations in **6m**, and at coplanar conformations for **7m**. The rotation barrier in both cases was found to be close to 1.4 kcal/mol. This difference was attributed to the lower energy level of the Cd 4d-orbitals, which allow them to participate more effectively in the conjugation with both $\pi$-systems of the oxime ligands. This conformational energy preference is fairly small, but apparently sufficient to result in different packing modes of analogous complexes in crystal.

Dissimilarities in the crystal packing of CPs **1**−**4** primarily revealed in their crystallization in different space groups, for example, compounds **1**, **3**, and **4** crystallize in the centrosymmetric *Pbca*, $P2_1/c$, and *Pnma* space groups, while compound **2** crystallizes in the acentric monoclinic $P2_1$ space group (Table 1). The structure extensions through the sulfate bridges generate the helical chains (Figure 2) with the metal···metal separations of


dx.doi.org/10.1021/jp5007395 | J. Phys. Chem. C 2014, 118, 9217−9227

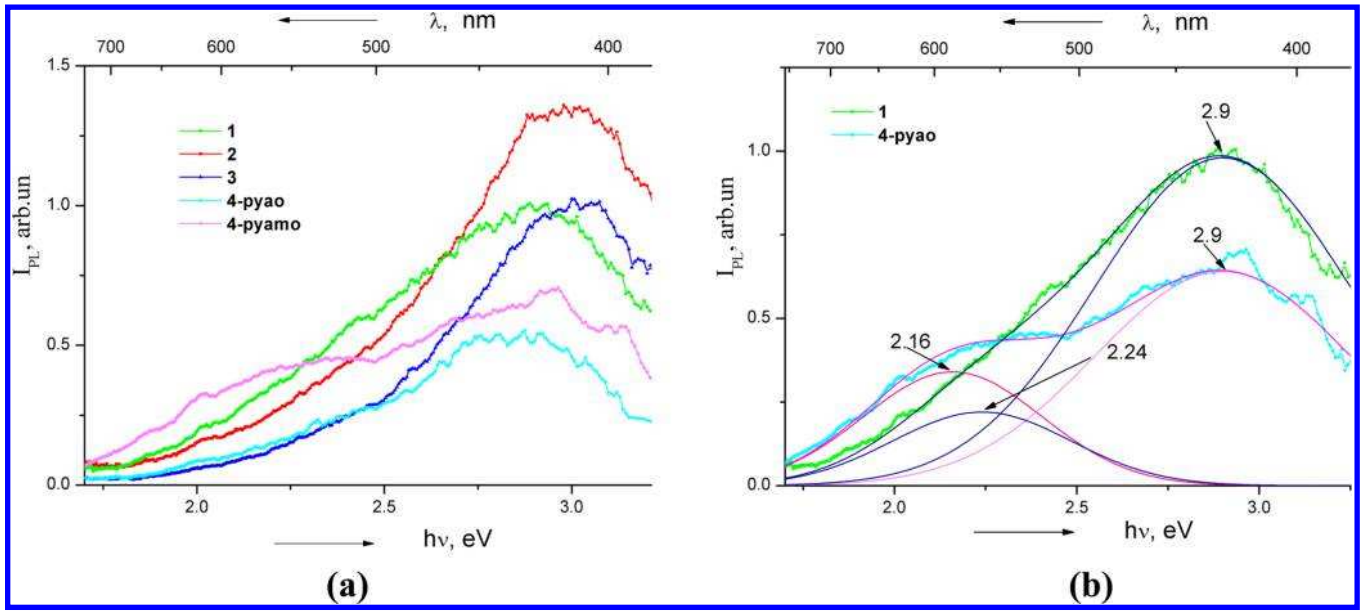


**Figure 3.** (a) Emission spectra for **1**−**3** and pure 4-pyao and 4-pyamo ligands. (b) Deconvolution of emission bands for 4-pyao ligand and coordination polymer **1**.

5.284 Å in **1**, 6.005 Å in **2**, 5.483 Å in **3**, and 5.369 Å in **4**. The organization of chains is rather similar in the centrosymmetric structures **1**, **3**, and **4**, with the T-shape arrangements of the oxime molecules at the neighboring metal centers within the chains, and dissimilar in **2**, with the overlapping of practically parallel neighboring 4-pyao molecules within the chain (Figure 2c, d). This difference is also reflected in the metal···metal separation of 6.005 Å in **2** being maximal within this series.

The luminescence for the 1D polymers **1**−**3**, and the 4-pyao and 4-pyamo ligands was studied in the solid state upon excitation at 355 nm (Figure 3). Similar to the recently reported by us pyridine-2-aldoxime-based polymeric Zn(II) and Cd(II) sulfates,[43] the emission of 1D polymers **1**−**3** displays apparently ligand-based, as the positions of emission maxima remain practically unchanged from free ligands to complexes. The more detailed inspection of emission curves for 4-pyao ligand and polymeric material **1** reveals their dual fluorescence in the solid state (Figure 3b). The Gaussian method was employed for spectrum resolution herein,[91,92] and the shapes of the emission curves indicate superposition of at least two bands with peaks at 2.90 eV (420 nm) and 2.16 eV (575 nm). Similar to our previous results, these emissions might be assigned to the $S_1$ and $S_2$ lowest excited states of the ligand, with first one being of the $\pi-\pi^*$ type (with respect to the 4-pyao molecular plane), and the second one of $n-\pi^*$ type connected with the electron removal from the lone pair of the pyridine N atom. Since both states are assigned to the 4-pyao ligand, the nature of the metal atom does not affect the wavelengths of this dual fluorescence, in agreement with the experimental data (Figure 3a). The enhancement of luminescence in polymers in comparison with the pure ligands may be attributed to the chelation of the ligand to the metal center. This enhances the rigidity of the ligand and thus reduces the loss of energy through a radiationless pathway.[93]

The pyridine-4-aldoxime was recently used as a component of the mixed crystal with efficient second harmonic generation NLO property.[94] Since some of the crystals reported in this contribution belong to the centrosymmetric space groups, the second order nonlinearities vanish in crystals **1**, **3**, and **4** but can be observed in crystals **2** and **5** that belong to the acentric space groups ($P2_1$ and $P2_12_12_1$). However, the optical nonlinearity of all the crystals studied may reveal itself in the third order of external field, such as the two photon absorption. Simultaneous absorption of two photons have important technological implications such as optical power limiting,[73] up-conversion lasing,[95] and chemical and biological sensing.[96,84] However, 2PA process has a relatively low probability, and molecular design, leading to enhancement of 2PA cross sections attracting considerable interest. Recently, Cd-,[33] Zn-,[97,98] Ru-,[99] and Pt-based[100] MOMs had been reported. One may therefore raise a reasonable question on whether crystals **1**−**5** may be found to be efficient two-photon absorbing materials.

Here, we used the structure of the crystals **1**−**5** in order to answer this question, and, perhaps, more importantly, to formulate the principles of MOM optimization for the purposes of enhancing their nonlinear optical properties. Before we present our estimates for the crystals **1**−**5**, one has to note that experimental investigation of 2PA spectra presents considerable challenge.[101] For that reason, such investigation extends beyond the scope of present work. Also, one has to be careful when selecting the representative fragment of the crystal for the purposes of 2PA spectra prediction, as crystalline environment may affect the NLO properties. Some of us investigated the effect of the environment both experimentally[35] and theoretically[102,103] and found that stacking interactions of the conjugated $\pi$-systems, leading to H-aggregation[36] in the solid state, affect the optical properties to a much greater degree than the herringbone (T-shaped) interactions of the phenyl rings. Among the structures reported in this work, the largest stacking overlap is found in crystal **5**. Comparison of 2PA cross sections for the monomeric complex and their stacking dimer found in the crystals of **5** demonstrates insignificant shifts in both pick position and this height. For this reason, we only report 2PA results for the monomeric complexes in crystals **1**−**5** in Table 2.

As one can see from the Table 2, two-photon absorption cross sections of the complexes **1m**−**5m** is in the range of 18−25 GM, similar to that of green fluorescent protein chromophore.[104] These values present considerable enhancement compared to 2PA cross sections of the 4-pyao and 4-pyamo ligands (3 and 6


dx.doi.org/10.1021/jp5007395 | J. Phys. Chem. C 2014, 118, 9217−9227

**Table 2. Properties of the Monomer Complexes 1m−5m, Free Ligands 4-Pyao and 4-Pyamo, as Well as the Model Complexes Calculated at TD-DFT Level with Three Exchange-Correlation Functionals: M05-QX, B3LYP, and CAM-B3LYP[a]**

| model system | $\sigma$ | $E$ | $\lambda$ | $\mu$(gf) | $\Delta\mu$(f) | $\mu$(gi) | $\mu$(if) |
|---|---|---|---|---|---|---|---|
| | | | M05-QX | | | | |
| 4-pyao | 3 | 5.00 | 248 | 1.12 | 0.3 | 1.72 | 0.84 |
| 4-pyamo | 6 | 4.51 | 275 | 1.23 | 2.28 | 0.26 | 0.88 |
| $[Zn(4\text{-pyao})(H_2O)_5]$ | 10 | 4.82 | 257 | 2.15 | 1.78 | | |
| $[Cd(4\text{-pyao})(H_2O)_5]$ | 11 | 4.88 | 254 | 2.14 | 1.98 | | |
| $[Zn(4\text{-pyamo})(H_2O)_5]$ | 12 | 3.71 | 334 | 1.35 | 2.93 | | |
| $[Cd(4\text{-pyamo})(H_2O)_5]$ | 12 | 3.95 | 314 | 1.24 | 2.98 | | |
| **1m** | 22 | 4.87 | 255 | | | | |
| **2m** | 13 | 4.69 | 264 | | | | |
| | 16 | 4.90 | 253 | | | | |
| **3m** | 12 | 3.75 | 331 | | | | |
| | 14 | 3.92 | 316 | | | | |
| **4m** | 26 | 4.05 | 306 | | | | |
| **5m** | 10 | 3.99 | 311 | | | | |
| | 14 | 4.10 | 302 | | | | |
| | | | B3LYP | | | | |
| **1m** | 27 | 4.67 | 266 | | | | |
| **2m** | 20 | 4.47 | 277 | | | | |
| | 18 | 4.69 | 264 | | | | |
| **3m** | 9 | 3.43 | 362 | | | | |
| | 19 | 3.60 | 344 | | | | |
| **4m** | 24 | 3.62 | 342 | | | | |
| **5m** | 12 | 3.59 | 346 | | | | |
| | 15 | 3.69 | 336 | | | | |
| | | | CAM-B3LYP | | | | |
| **1m** | 15 | 5.04 | 246 | | | | |
| **2m** | 9 | 4.84 | 256 | | | | |
| | 11 | 5.07 | 245 | | | | |
| **3m** | 11 | 4.21 | 294 | | | | |
| | 15 | 4.31 | 288 | | | | |
| **4m** | 21 | 4.39 | 282 | | | | |
| **5m** | 11 | 4.33 | 287 | | | | |
| | 13 | 4.44 | 279 | | | | |

[a]The 2PA cross sections $\sigma$ (in GM), excitation energies $E$ (in eV), and absorption wavelengths $\lambda$ (in nm) are reported. Also shown are the permanent dipole moments difference between 2PA absorbing (final, f) and ground (g) states, as well as transition dipole moments $\mu$ (in atomic units) from the ground to final, ground to intermediate (i, one photon absorbing) state, and intermediate to final states, respectively.

GM, respectively). Comparison with the model complexes shows that if one of the two organic ligands is substituted with the water molecule, 2PA efficiency is reduced by half, and still exceeds the 2PA cross section of the isolated ligand by 2−3-fold. In order to further investigate the origin of this enhancement, we analyzed 4-pyamo in greater details. The HOMO−LUMO transition in this molecule corresponds to the singlet excited state with large oscillator strength and 2PA cross section. According to two-state model for the polar chromophores, this cross section is proportional to the squared change of the permanent dipole moment upon excitation and squared transition dipole moment to the ground state. These permanent and transition dipole moments are also listed in Table 2. After Zn(II) coordination, the LUMO remains localized on the ligand, but it is somewhat destabilized and polarized toward the metal, so that the dipole moment change upon excitation is increased from 2.3 and 2.9 D. As the result, the resonant 2PA cross section of this state nearly doubles. Addition of the second ligand in orthogonal conformation and formation of the complex **3m** results in appearance of another, nearly degenerate state, localized on this added ligand, with a similar 2PA cross section. The two peaks overlap on 2PA spectrum and increase the resulting cross section by ∼50%. The situation is somewhat different for the complex **4m**, however. Here the essential states, localized on two ligands, mix. Resulting symmetric combination has high oscillator strength and is somewhat stabilized. Antisymmetric combination, on the other hand, has zero oscillator strength and is slightly destabilized in energy (J-aggregate type state coupling). According to the three-state model for symmetric chromophores, 2PA cross section for this state is proportional to the squared product of two transition dipole moments: one between ground to intermediate 1PA state, and another one is 1PA to the final 2PA state. Resulting 2PA cross section of antisymmetric combination more than doubles compared to the initial ligand-localized states.

In order to test sensitivity of out 2PA predictions to the exchange-correlation functional used, we report the results obtained with widely used functionals B3LYP and CAM-B3LYP in Table 2 as well. The functionals contain 20% and up to 60% of the Hartree−Fock exchange, respectively, as compared to 35% of Hartree−Fock exchange in M05-QX. One can see that B3LYP and CAM-B3LYP shift the 2PA resonance almost uniformly (by ∼10 nm) to the longer and shorter wavelengths, respectively. The 2PA cross sections are also increased or decreased by ∼25%,


dx.doi.org/10.1021/jp5007395 | J. Phys. Chem. C 2014, 118, 9217−9227

and (in the case of two 2PA bands) their intensity is slightly redistributed. These variations, however, do not change our quantitative conclusions on the mechanisms of 2PA enhancements upon the complex formation.

## CONCLUSIONS

Four mixed-ligand 1D coordination polymers, $[Zn(SO_4)(4\text{-pyao})_2(H_2O)_2]_n$ **1**, $[Cd(SO_4)(4\text{-pyao})_2(H_2O)_2]_n$ **2**, $[Zn(SO_4)(4\text{-pyamo})_2(H_2O)_2]_n$ **3**, and $[Cd(SO_4)(4\text{-pyamo})_2(H_2O)_2]_n$ **4**, and mononuclear complex $[Zn(SO_4)(4\text{-pyamo})_2(H_2O)_3]$ **5** have been prepared, and their crystal structure and spectra were analyzed. The coordination polymers **1**−**4** represent supramolecular conformational isomers distinguishing by the restricting rotation of the neutral 4-pyao/4-pyamo ligands along the metal centers, and crystallizing in the different space groups. The four 1D coordination polymers form pairs, identical in compositions materials, and represent supramolecular isomers that only differ by the arrangement of two oxime molecules coordinated to the metal centers. The distinctions in the nature of the metal makes more pronounced impact on structural dissimilarities, than substitution effect in oxime ligand.

The complexes are further investigated as potential two-photon absorbing chromophores. TD-DFT calculations predict that metal coordination considerably enhances nonlinear optical response of the conjugated ligands. Detailed analyses of the electronic structure reveals the mechanism of this enhancement. Metal coordination polarizes the LUMO, increasing the permanent dipole moment of the excited state, and its 2PA cross section. Coplanar coordination of the two ligands in Cd(II) complex more than doubles the 2PA cross section due to J-aggregate type state coupling. Nonplanar conformation of the two ligands in Zn(II) complexes results in less pronounced enhancement of NLO properties.

Our continuous efforts are aimed at the further modifications of these solids by consecutive substitution of water molecules by sulfate ligands in the metal coordination environment, that being in line with our previous findings.[29,43] Computational predictions reported herein, should assist in design of new coordination polymers with expected nonlinear optical properties. Coordination polymers **1**−**3** also reveal ligand-based luminescence properties in the solid state.

## ASSOCIATED CONTENT

### Supporting Information

Synthetic procedures, IR spectra, selected bond distances, and full crystallographic data in cif format for **1**−**5**. This material is available free of charge via the Internet at http://pubs.acs.org. Crystallographic data for new structures reported herein were deposited with the Cambridge Crystallographic Data Centre and allocated the deposition numbers CCDC 988203−988207. These data can be obtained free of charge from the Cambridge Crystallographic Data Centre via www.ccdc.cam.ac.uk/data_request/cif.

## AUTHOR INFORMATION

### Corresponding Authors

*(A.E.M.) Phone: 407-374-3783. E-mail: amasunov@ucf.edu.
*(M.S.F.) Fax: 373 22 725887. E-mail: fonari.xray@phys.asm.md.

### Notes

The authors declare no competing financial interest.

## ACKNOWLEDGMENTS

This work was supported in part by the U.S. National Science Foundation (CHE-0832622). H.J.R.-J. and A.E.M. acknowledge the use of computational resources at The Stokes Advanced Research Computing Center, University of Central Florida (UCF), and the National Energy Research Scientific Computing Center, which is supported by the Office of Science of the U.S. Department of Energy under Contract No. DE-AC02-05CH11231.

## REFERENCES

(1) Cui, Y.; Yue, Y.; Qian, G.; Chen, B. Luminescent Functional Metal-Organic Frameworks. *Chem. Rev.* **2012**, *112*, 1126−1162.
(2) Cunha, D.; Ben Yahia, M.; Hall, S.; Miller, S. R.; Chevreau, H.; Elkaim, E.; Maurin, G.; Horcajada, P.; Serre, C. Rationale of Drug Encapsulation and Release from Biocompatible Porous Metal-Organic Frameworks. *Chem. Mater.* **2013**, *25*, 2767−2776.
(3) Eddaoudi, M.; Moler, D. B.; Li, H. L.; Chen, B. L.; Reineke, T. M.; O'Keeffe, M.; Yaghi, O. M. Modular Chemistry: Secondary Building Units as a Basis for the Design of Highly Porous and Robust Metal-Organic Carboxylate Frameworks. *Acc. Chem. Res.* **2001**, *34*, 319−330.
(4) Janiak, C. Engineering Coordination Polymers Towards Applications. *Dalton Trans.* **2003**, 2781−2804.
(5) Horike, S.; Kitagawa, S. Design of Porous Coordination Polymers/Metal−Organic Frameworks: Past, Present and Future. In *Metal-Organic Frameworks: Applications from Catalysis to Gas Storage*; Wiley-VCH Verlag GmbH & Co. KgaA: Berlin, 2011.
(6) Kreno, L. E.; Leong, K.; Farha, O. K.; Allendorf, M.; Van Duyne, R. P.; Hupp, J. T. Metal-Organic Framework Materials as Chemical Sensors. *Chem. Rev.* **2012**, *112*, 1105−1125.
(7) Robin, A. Y.; Fromm, K. M. Coordination Polymer Networks with O- and N-Donors: What They Are, Why and How They Are Made. *Coord. Chem. Rev.* **2006**, *250*, 2127−2157.
(8) Erxleben, A. Structures and Properties of Zn(II) Coordination Polymers. *Coord. Chem. Rev.* **2003**, *246*, 203−228.
(9) Liu, H.-Y.; Ma, J.-F.; Liu, Y.-Y.; Yang, J. A Series of Zn(II) and Cd(II) Coordination Polymers Based on Flexible Bis-(pyridyl)-benzimidazole Ligand and Different Carboxylates: Syntheses, Structures, and Photoluminescent Properties. *CrystEngComm* **2013**, *15*, 2699−2708.
(10) Lu, W. G.; Jiang, L.; Feng, X. L.; Lu, T. B. Three 3D Coordination Polymers Constructed by Cd(II) and Zn(II) with Imidazole-4,5-dicarboxylate and 4,4′-Bipyridyl Building Blocks. *Cryst. Growth Des.* **2006**, *6*, 564−571.
(11) Wang, L.; You, W.; Huang, W.; Wang, C.; You, X.-Z. Alteration of Molecular Conformations, Coordination Modes, and Architectures for a Novel 3,8-Diimidazol-1,10-phenanthroline Compound in the Construction of Cadmium(II) and Zinc(II) Homochiral Coordination Polymers Involving an Auxiliary Chiral Camphorate Ligand. *Inorg. Chem.* **2009**, *48*, 4295−4305.
(12) Withersby, M. A.; Blake, A. J.; Champness, N. R.; Cooke, P. A.; Hubberstey, P.; Li, W. S.; Schroder, M. Solvent Control in the Synthesis of 3,6-Bis(pyridin-3-yl)-1,2,4,5-tetrazine-bridged Cadmium(II) and Zinc(II) Coordination Polymers. *Inorg. Chem.* **1999**, *38*, 2259−2266.
(13) Yoshida, J.; Nishikiori, S.-i.; Kuroda, R.; Yuge, H. Three Polymorphic Cd(II) Coordination Polymers Obtained from the Solution and Mechanochemical Reactions of 3-Cyanopentane-2,4-dione with Cd(II) Acetate. *Chem.—Eur. J.* **2013**, *19*, 3451−3457.
(14) Bu, X. H.; Chen, W.; Lu, S. L.; Zhang, R. H.; Liao, D. Z.; Bu, W. M.; Shionoya, M.; Brisse, F.; Ribas, J. Flexible *meso*-Bis(sulfinyl) Ligands as Building Blocks for Copper(II) Coordination Polymers: Cavity Control by Varying the Chain Length of Ligands. *Angew. Chem.* **2001**, *113*, 3301−3303.
(15) Carlucci, L.; Ciani, G.; Proserpio, D. M.; Rizzato, S. Coordination Networks from the Self-assembly of Silver Salts and the Linear Chain Dinitriles $NC(CH_2)(n)CN$ (n = 2 to 7): a Systematic Investigation of

the Role of Counterions and of the Increasing Length of the Spacers. *CrystEngComm* **2002**, 413−425.
(16) Wang, X. L.; Chao, Q.; Wang, E. B.; Lin, X.; Su, Z. M.; Hu, C. W. Interlocked and Interdigitated Architectures from Self-assembly of Long Flexible Ligands and Cadmium Salts. *Angew. Chem., Int. Ed.* **2004**, *43*, 5036−5040.
(17) Moulton, B.; Zaworotko, M. J. From Molecules to Crystal Engineering: Supramolecular Isomerism and Polymorphism in Network Solids. *Chem. Rev.* **2001**, *101*, 1629−1658.
(18) Abourahma, H.; Moulton, B.; Kravtsov, V.; Zaworotko, M. J. Supramolecular Isomerism in Coordination Compounds: Nanoscale Molecular Hexagons and Chains. *J. Am. Chem. Soc.* **2002**, *124*, 9990−9991.
(19) Bourne, S. A. *Supramolecular Chemistry: From Molecules to Nanomaterials*; John Wiley & Sons: New York, 2012.
(20) Deng, D.; Liu, L.; Ji, B.-M.; Yin, G.; Du, C. Temperature, Cooling Rate, and Additive-Controlled Supramolecular Isomerism in Four Pb(II) Coordination Polymers with an in Situ Ligand Transformation Reaction. *Cryst. Growth Des.* **2012**, *12*, 5338−5348.
(21) Hennigar, T. L.; MacQuarrie, D. C.; Losier, P.; Rogers, R. D.; Zaworotko, M. J. Supramolecular Isomerism in Coordination Polymers: Conformational Freedom of Ligands in $[Co(NO_3)_2(1,2\text{-bis}(4\text{-pyridyl})\text{-ethane})_{1.5}]_n$. *Angew. Chem., Int. Ed.* **1997**, *36*, 972−973.
(22) Zhang, J.-P.; Huang, X.-C.; Chen, X.-M. Supramolecular Isomerism in Coordination Polymers. *Chem. Soc. Rev.* **2009**, *38*, 2385−2396.
(23) Tong, M. L.; Hu, S.; Wang, J.; Kitagawa, S.; Ng, S. W. Supramolecular Isomerism in Cadmium Hydroxide Phases. Temperature-dependent Synthesis and Structure of Photoluminescent Coordination Polymers of alpha- and beta-Cd-2(OH)(2)(2,4-pyda). *Cryst. Growth Des.* **2005**, *5*, 837−839.
(24) Tian, Z.; Lin, J.; Su, Y.; Wen, L.; Liu, Y.; Zhu, H.; Meng, Q.-J. Flexible Ligand, Structural, and Topological Diversity: Isomerism in $Zn(NO_3)_2$ Coordination Polymers. *Cryst. Growth Des.* **2007**, *7*, 1863−1867.
(25) Cui, P.; Wu, J.; Zhao, X.; Sun, D.; Zhang, L.; Guo, J.; Sun, D. Two Solvent-Dependent Zinc(II) Supramolecular Isomers: Rare kgd and Lonsdaleite Network Topologies Based on a Tripodal Flexible Ligand. *Cryst. Growth Des.* **2011**, *11*, 5182−5187.
(26) Chen, D.-S.; Sun, L.-B.; Liang, Z.-Q.; Shao, K.-Z.; Wang, C.-G.; Su, Z.-M.; Xing, H.-Z. Conformational Supramolecular Isomerism in Two-Dimensional Fluorescent Coordination Polymers Based on Flexible Tetracarboxylate Ligand. *Cryst. Growth Des.* **2013**, *13*, 4092−4099.
(27) Tan, Y. S.; Sudlow, A. L.; Molloy, K. C.; Morishima, Y.; Fujisawa, K.; Jackson, W. J.; Henderson, W.; Halim, S. N. B. A.; Ng, S. W.; Tiekink, E. R. T. Supramolecular Isomerism in a Cadmium Bis(N-Hydroxyethyl, N-isopropyldithiocarbamate) Compound: Physiochemical Characterization of Ball (n=2) and Chain (n = infinity) Forms of $\{Cd[S_2CN(iPr)CH_2CH_2OH]_2\cdot\text{solvent}\}_n$. *Cryst. Growth Des.* **2013**, *13*, 3046−3056.
(28) Croitor, L.; Coropceanu, E. B.; Jeanneau, E.; Dementiev, I. V.; Goglidze, T. I.; Chumakov, Y. M.; Fonari, M. S. Anion-Induced Generation of Binuclear and Polymeric Cd(II) and Zn(II) Coordination Compounds with 4,4 ′-Bipyridine and Dioxime Ligands. *Cryst. Growth Des.* **2009**, *9*, 5233−5243.
(29) Croitor, L.; Coropceanu, E. B.; Siminel, A. V.; Kravtsov, V. C.; Fonari, M. S. Polymeric Zn(II) and Cd(II) Sulfates with Bipyridine and Dioxime Ligands: Supramolecular Isomerism, Chirality, and Luminescence. *Cryst. Growth Des.* **2011**, *11*, 3536−3544.
(30) Croitor, L.; Coropceanu, E. B.; Siminel, A. V.; Kulikova, O.; Zelentsov, V. I.; Datsko, T.; Fonari, M. S. 1,2-Cyclohexanedionedioxime as a Useful Co-Ligand for Fabrication of One-dimensional Zn(II) and Cd(II) Coordination Polymers with Wheel-and-Axle Topology and Luminescent Properties. *CrystEngComm* **2012**, *14*, 3750−3758.
(31) Yu, J.; Cui, Y.; Xu, H.; Yang, Y.; Wang, Z.; Chen, B.; Qian, G. Confinement of Pyridinium Hemicyanine Dye within an Anionic Metal-Organic Framework for Two-Photon-Pumped Lasing. *Nat. Commun.* **2013**, *4*, 2719.
(32) Nie, C.; Zhang, Q.; Ding, H.; Huang, B.; Wang, X.; Zhao, X.; Li, S.; Zhou, H.; Wu, J.; Tian, Y. Two Novel Six-coordinated Cadmium(II) and Zinc(II) Complexes from Carbazate beta-Diketonate: Crystal Structures, Enhanced Two-Photon Absorption and Biological Imaging Application. *Dalton Trans.* **2014**, *43*, 599−608.
(33) Xu, D.; Yang, M.; Wang, Y.; Cao, Y.; Fang, M.; Zhu, W.; Zhou, H.; Hao, F.; Wu, J.; Tian, Y. New Dyes with Enhanced Two-Photon Absorption Cross-sections Based on the Cd(II) and 4-(4−4-(imidazole)styryl phenyl)-2,2:6,2-terpyridine. *J. Coord. Chem.* **2013**, *66*, 2992−3003.
(34) Coropceanu, E. B.; Croitor, L.; Siminel, A. V.; Fonari, M. S. Preparation, structural characterization and luminescence studies of mono- and binuclear Zn(II) and Cd(II) acetates with pyridine-4-aldoxime and pyridine-4-amidoxime ligands. *Polyhedron* **2014**, *75*, 73−80.
(35) Hu, H.; Fishman, D. A.; Gerasov, A. O.; Przhonska, O. V.; Webster, S.; Padilha, L. A.; Peceli, D.; Shandura, M.; Kovtun, Y. P.; Kachkovski, A. D.; et al. Two-Photon Absorption Spectrum of a Single Crystal Cyanine-like Dye. *J. Phys. Chem. Lett.* **2012**, *3*, 1222−1228.
(36) Passier, R.; Ritchie, J. P.; Toro, C.; Diaz, C.; Masunov, A. E.; Belfield, K. D.; Hernandez, F. E. Thermally Controlled Preferential Molecular Aggregation State in a Thiacarbocyanine Dye. *J. Chem. Phys.* **2010**, *133*, 134508−1−134508−7.
(37) Olesiak-Banska, J.; Matczyszyn, K.; Zalesny, R.; Murugan, N. A.; Kongsted, J.; Agren, H.; Bartkowiak, W.; Samoc, M. Revealing Spectral Features in Two-Photon Absorption Spectrum of Hoechst 33342: A Combined Experimental and Quantum-Chemical Study. *J. Phys. Chem. B* **2013**, *117*, 12013−12019.
(38) Papaefstathiou, G. S.; Escuer, A.; Mautner, F. A.; Raptopoulou, C.; Terzis, A.; Perlepes, S. P.; Vicente, R. Use of the Di-2-Pyridyl Ketone/Acetate/Dicyanamide ″Blend″ in Manganese(II), Cobalt(II) and Nickel(II) Chemistry: Neutral Cubane Complexes. *Eur. J. Inorg. Chem.* **2005**, 879−893.
(39) Stamatatos, T. C.; Diamantopoulou, E.; Raptopoulou, C. P.; Psycharis, V.; Escuer, A.; Perlepes, S. P. Acetate/di-2-Pyridyl Ketone Oximate "Blend" as a Source of High-Nuclearity Nickel(II) Clusters: Dependence of the Nuclearity on the Nature of the Inorganic Anion Present. *Inorg. Chem.* **2007**, *46*, 2350−2352.
(40) Coropceanu, E. B.; Croitor, L.; Siminel, A. V.; Fonari, M. S. Unique Tetranuclear Heterometallic Compound $[Na_2Zn_2\{(4\text{-py})C(H)(NOH)\}_2(CH_3COO)_6(H_2O)_4]\cdot 2H_2O$ with Luminescent Properties. *Inorg. Chem. Commun.* **2011**, *14*, 1528−1531.
(41) Croitor, L.; Coropceanu, E. B.; Siminel, A. V.; Botoshansky, M. M.; Fonari, M. S. Synthesis, Structures, and Luminescence Properties of Mixed Ligand Cd(II) and Zn(II) Coordination Compounds Mediated by 1,2-bis(4-Pyridyl)ethane. *Inorg. Chim. Acta* **2011**, *370*, 411−419.
(42) Coropceanu, E. B.; Croitor, L.; Fonari, M. S. Mononuclear Cd(II) and Zn(II) Complexes with the 1,2-Cyclohexanedionedioxime Ligand: Preparation and Structural Characterization. *Polyhedron* **2012**, *38*, 68−74.
(43) Croitor, L.; Coropceanu, E. B.; Siminel, A. V.; Masunov, A. E.; Fonari, M. S. From Discrete Molecules to One-Dimensional Coordination Polymers Containing Mn(II), Zn(II) or Cd(II) Pyridine-2-aldoxime Building Unit. *Polyhedron* **2013**, *60*, 140−150.
(44) Tamasi, G.; Cini, R. Study of Binary and Ternary Metal Complexes Containing the Sulfato Ligand: Molecular Models for Selected Non-Catalytic Sites in Sulfurylase. *Dalton Trans* **2003**, 2928−2936.
(45) Aakeroy, C. B.; Beatty, A. M.; Leinen, D. S. A Versatile Route to Porous Solids: Organic-Inorganic Hybrid Materials Assembled Through Hydrogen Bonds. *Angew. Chem., Int. Ed.* **1999**, *38*, 1815−1819.
(46) Zhang, B. F.; Chu, S.; Wang, X. Q.; Shen, G. Q.; Wang, R. J. An Adduct of (1,10-Phenanthroline)-diperchloratobis(pyridine-4-carboxaldehyde oxime-kappa N-1)copper(II) and Pyridine-4-carboxaldehyde oxime. *Acta Crystallogr.* **2003**, *E59*, M824−M826.
(47) Adams, C. J.; Crawford, P. C.; Orpen, A. G.; Podesta, T. J. Cation and Anion Diversity in $[M(\text{dithiooxalate})_2]^{2-}$ Salts: Structure Robustness in Crystal Synthesis. *Dalton Trans.* **2006**, 4078−4092.

(48) Kawasaki, T.; Kachi-Terajima, C.; Saito, T.; Kitazawa, T. Triply interpenetrated structure of $(Mn^{II}(L)_2[Ag^{I}(CN)_2]_2)\cdot(Mn^{II}(H_2O)_2[Ag^{I}(CN)_2]_2)$ (L = 4-CNpy or py-4-aldoxime). *Bull. Chem. Soc. Jpn.* **2008**, *81*, 268−273.
(49) Kawasaki, T.; Kitazawa, T. Dioxidobis(pentane-2,4-dionato-kappa$^2$*O*,*O*′)(pyridine-4-carbaldehyde oxime-kappa*N*$^1$)uranium(VI). *Acta Crystallogr.* **2008**, *E64*, M788.
(50) Mutambi, E. M. Aqua[4-(hydroxyiminomethyl)pyridine-kappa$^1$]-(pyridine-2,6-dicarboxylato-kappa$^3$*O*$^2$,*N*,*O*$^6$)copper(II). *Acta Crystallogr.* **2008**, *E64*, M979−M980.
(51) Konidaris, K. F.; Kaplanis, M.; Raptopoulou, C. P.; Perlepes, S. P.; Manessi-Zoupa, E.; Katsoulakou, E. Dinuclear Versus Trinuclear Complex Formation in Zinc(II) Benzoate/Pyridyl Oxime Chemistry Depending on the Position of the Oxime Group. *Polyhedron* **2009**, *28*, 3243−3250.
(52) Ohkoshi, S.-i.; Imoto, K.; Tsunobuchi, Y.; Takano, S.; Tokoro, H. Light-Induced Spin-Crossover Magnet. *Nat. Chem.* **2011**, *3*, 564−569.
(53) Yang, Y.; Chai, W.; Song, L.; Yang, Y.; Chen, J. Aqua[4-(hydroxyiminomethyl)pyridine-kappa*N*$^1$](iminodiacetato-kappa$^3$*O*,*N*,*O*′)copper(II). *Acta Crystallogr.* **2011**, *E67*, M1291−M1292.
(54) Nandy, M.; Banerjee, S.; Rizzoli, C.; Zangrando, E.; Nonat, A.; Charbonnière, L. J.; Mitra, S. Syntheses, Structural Diversity and Photo-Physical Properties of Copper(I) and Silver(I) Coordination Polymers Based on the Pyridine-4-amidoxime Ligand. *Polyhedron* **2013**, *65*, 252−261.
(55) Sheldrick, G. M. A Short History of SHELX. *Acta Crystallogr.* **2008**, *A64*, 112−122.
(56) Macrae, C. F.; Edgington, P. R.; McCabe, P.; Pidcock, E.; Shields, G. P.; Taylor, R.; Towler, M.; van De Streek, J. Mercury: Visualization and Analysis of Crystal Structures. *J. Appl. Crystallogr.* **2006**, *39*, 453−457.
(57) Frisch, M. J. et al. *Gaussian 09*, Revision D.01; Gaussian Inc.: Wallingford, CT, 2009.
(58) Mikhailov, I. A.; Bondar, M. V.; Belfield, K. D.; Masunov, A. E. Electronic Properties of a New Two-Photon Absorbing Fluorene Derivative: The Role of Hartree-Fock Exchange in the Density Functional Theory Design of Improved Nonlinear Chromophores. *J. Phys. Chem. C* **2009**, *113*, 20719−20724.
(59) Zhao, Y.; Schultz, N. E.; Truhlar, D. G. Design of Density Functionals by Combining the Method of Constraint Satisfaction with Parametrization for Thermochemistry, Thermochemical Kinetics, and Noncovalent Interactions. *J. Chem. Theory Comput.* **2006**, *2*, 364−382.
(60) Andrae, D.; Haussermann, U.; Dolg, M.; Stoll, H.; Preuss, H. Energy-Adjusted Ab Initio Pseudopotentials for the 2nd and 3rd row Transition-Elements. *Theor. Chim. Acta* **1990**, *77*, 123−141.
(61) Dunning, T. H., Jr.; Hay, P. J. *Modern Theoretical Chemistry*; Schaefer, H. F., III, Ed.; Plenum: New York, 1977; Vol. 3, pp 1−21.
(62) Casida, M. E.; Huix-Rotllant, M. Progress in Time-Dependent Density-Functional Theory. *Annu. Rev. Phys. Chem.* **2012**, *63*, 287−323.
(63) Masunov, A. E. Theoretical Spectroscopy of Carbocyanine Dyes Made Accurate by Frozen Density Correction to Excitation Energies Obtained by TD-DFT. *Int. J. Quantum Chem.* **2010**, *110*, 3095−3100.
(64) Jacquemin, D.; Mennucci, B.; Adamo, C. Excited-state Calculations with TD-DFT: from Benchmarks to Simulations in Complex Environments. *Phys. Chem. Chem. Phys.* **2011**, *13*, 16987−16998.
(65) Laurent, A. D.; Jacquemin, D. TD-DFT Benchmarks: A review. *Int. J. Quantum Chem.* **2013**, *113*, 2019−2039.
(66) Masunov, A.; Tretiak, S.; Hong, J. W.; Liu, B.; Bazan, G. C. Theoretical Study of the Effects of Solvent Environment on Photophysical Properties and Electronic Structure of Paracyclophane Chromophores. *J. Chem. Phys.* **2005**, *122*, 224505−1−224505−10.
(67) Toro, C.; Thibert, A.; De Boni, L.; Masunov, A. E.; Hernandez, F. E. Fluorescence Emission of Disperse Red 1 in Solution at Room Temperature. *J. Phys. Chem. B* **2008**, *112*, 929−937.
(68) Moreshead, W. V.; Przhonska, O. V.; Bondar, M. V.; Kachkovsky, A. D.; Nayyar, I. H.; Masunov, A. E.; Woodward, A. D.; Belfield, K. D. Design of New Optical Material with Broad Spectrum Linear and Two-Photon Absorption and Solvatochromism. *J. Phys. Chem. C* **2013**, *117*, 23133−23147.
(69) Ganin, E. V.; Masunov, A. E.; Siminel, A. V.; Fonari, M. S. Preparation, Characterization, and Electronic Structure of Asymmetric Isonaphthalimide: Mechanism of Dual Fluorescence in Solid State. *J. Phys. Chem. C* **2013**, *117*, 18154−18162.
(70) De Boni, L.; Toro, C.; Masunov, A. E.; Hernandez, F. E. Untangling the Excited States of DR1 in Solution: An Experimental and Theoretical Study. *J. Phys. Chem. A* **2008**, *112*, 3886−3890.
(71) Patel, P. D.; Mikhailov, I. A.; Belfield, K. D.; Masunov, A. E. Theoretical Study of Photochromic Compounds, Part 2: Thermal Mechanism for Byproduct Formation and Fatigue Resistance of Diarylethenes Used as Data Storage Materials. *Int. J. Quantum Chem.* **2009**, *109*, 3711−3722.
(72) Mikhailov, I. A.; Belfield, K. D.; Masunov, A. E. DFT-Based Methods in the Design of Two-Photon Operated Molecular Switches. *J. Phys. Chem. A* **2009**, *113*, 7080−7089.
(73) Masunov, A. E.; Mikhailov, I. A. Theory and Computations of Two-Photon Absorbing Photochromic Chromophores. *Eur. J. Chem.* **2010**, *1*, 142−161.
(74) Liu, Y. J. Computational Photochemistry. *Prog. Chem.* **2012**, *24*, 950−956.
(75) Mikhailov, I. A.; Tafur, S.; Masunov, A. E. Double Excitations and State-to-State Transition Dipoles in $\pi-\pi^*$ Excited Singlet States of Linear Polyenes: Time-Dependent Density-Functional Theory Versus Multiconfigurational Methods. *Phys. Rev. A* **2008**, *77*, 012510−1−012510−11.
(76) Chernyak, V.; Mukamel, S. Density-Matrix Representation of Nonadiabatic Couplings in Time-Dependent Density Functional (TDDFT) Theories. *J. Chem. Phys.* **2000**, *112*, 3572−3579.
(77) Tretiak, S.; Mukamel, S. Density Matrix Analysis and Simulation of Electronic Excitations in Conjugated and Aggregated Molecules. *Chem. Rev.* **2002**, *102*, 3171−3212.
(78) Tretiak, S.; Chernyak, V. Resonant Nonlinear Polarizabilities in the Time-Dependent Density Functional Theory. *J. Chem. Phys.* **2003**, *119*, 8809−8823.
(79) Mikhailov, I. A.; Musial, M.; Masunov, A. E. Permanent Dipole Moments and Energies of Excited States from Density Functional Theory Compared with Coupled Cluster Predictions: Case of *para*-Nitroaniline. *Comput. Theor. Chem.* **2013**, *1019*, 23−32.
(80) Ohta, K.; Kamada, K. Theoretical Investigation of Two-Photon Absorption Allowed Excited States in Symmetrically Substituted Diacetylenes by Ab Initio Molecular-Orbital Method. *J. Chem. Phys.* **2006**, *124*, 124303−124311.
(81) Rumi, M.; Ehrlich, J. E.; Heikal, A. A.; Perry, J. W.; Barlow, S.; Hu, Z. Y.; McCord-Maughon, D.; Parker, T. C.; Rockel, H.; Thayumanavan, S.; et al. Structure-Property Relationships for Two-Photon Absorbing Chromophores: Bis-Donor Diphenylpolyene and Bis(styryl)benzene Derivatives. *J. Am. Chem. Soc.* **2000**, *122*, 9500−9510.
(82) Masunov, A. M.; Tretiak, S. Prediction of Two-Photon Absorption Properties for Organic Chromophores Using Time-Dependent Density-Functional Theory. *J. Phys. Chem. B* **2004**, *108*, 899−907.
(83) Nayyar, I. H.; Masunov, A. E.; Tretiak, S. Comparison of TD-DFT Methods for the Calculation of Two-Photon Absorption Spectra of Oligophenylvinylenes. *J. Phys. Chem. C* **2013**, *117*, 18170−18189.
(84) Belfield, K. D.; Bondar, M. V.; Frazer, A.; Morales, A. R.; Kachkovsky, O. D.; Mikhailov, I. A.; Masunov, A. E.; Przhonska, O. V. Fluorene-Based Metal-Ion Sensing Probe with High Sensitivity to $Zn^{2+}$ and Efficient Two-Photon Absorption. *J. Phys. Chem. B* **2010**, *114*, 9313−9321.
(85) Belfield, K. D.; Bondar, M. V.; Hernandez, F. E.; Masunov, A. E.; Mikhailov, I. A.; Morales, A. R.; Przhonska, O. V.; Yao, S. Two-Photon Absorption Properties of New Fluorene-Based Singlet Oxygen Photosensitizers. *J. Phys. Chem. C* **2009**, *113*, 4706−4711.
(86) Webster, S.; Peceli, D.; Hu, H.; Padilha, L. A.; Przhonska, O. V.; Masunov, A. E.; Gerasov, A. O.; Kachkovski, A. D.; Slominsky, Y. L.; Tolmachev, A. I.; et al. Near-Unity Quantum Yields for Intersystem Crossing and Singlet Oxygen Generation in Polymethine-like

Molecules: Design and Experimental Realization. *J. Phys. Chem. Lett.* **2010**, *1*, 2354−2360.
(87) Luchita, G.; Bondar, M. V.; Yao, S.; Mikhailov, I. A.; Yanez, C. O.; Przhonska, O. V.; Masunov, A. E.; Belfield, K. D. Efficient Photochromic Transformation of a New Fluorenyl Diarylethene: One- and Two-Photon Absorption Spectroscopy. *ACS Appl. Mater. Interfaces* **2011**, 3559−3567.
(88) Peceli, D.; Hu, H.; Fishman, D. A.; Webster, S.; Przhonska, O. V.; Kurdyukov, V. V.; Slominsky, Y. L.; Tolmachev, A. I.; Kachkovski, A. D.; Gerasov, A. O.; et al. Enhanced Intersystem Crossing Rate in Polymethine-Like Molecules: Sulfur-Containing Squaraines versus Oxygen-Containing Analogues. *J. Phys. Chem. A* **2013**, *117*, 2333−2346.
(89) Toro, C.; De Boni, L.; Yao, S.; Ritchie, J. P.; Masunov, A. E.; Belfield, K. D.; Hernandez, F. E. Linear and nonlinear optical characterization of a monomeric symmetric squaraine-based dye in solution. *J. Chem. Phys.* **2009**, *130*, 214504-1−214504-6.
(90) Kauffman, J. F.; Turner, J. M.; Alabugin, I. V.; Breiner, B.; Kovalenko, S. V.; Badaeva, E. A.; Masunov, A.; Tretiak, S. Two-photon excitation of substituted enediynes. *J. Phys. Chem. A* **2006**, *110*, 241−251.
(91) Sunshine, J. M.; Pieters, C. M.; Pratt, S. F. Deconvolution of Mineral Absorption-Bands - an Improved Approach. *J. Geophys. Res., [Solid Earth Planets]* **1990**, *95*, 6955−6966.
(92) Kuznetsov, V. N.; Ryabchuk, V. K.; Emeline, A. V.; Mikhaylov, R. V.; Rudakova, A. V.; Serpone, N. Thermo- and Photo-stimulated Effects on the Optical Properties of Rutile Titania Ceramic Layers Formed on Titanium Substrates. *Chem. Mater.* **2013**, *25*, 170−177.
(93) Zheng, S. L.; Yang, J. H.; Yu, X. L.; Chen, X. M.; Wong, W. T. Syntheses, Structures, Photoluminescence, and Theoretical Studies of $d^{10}$ Metal Complexes of 2,2′-Dihydroxy-1,1′-binaphthalenyl-3,3′-dicarboxylate. *Inorg. Chem.* **2004**, *43*, 830−838.
(94) Ivanova, B. B.; Spiteller, M. Optical and Nonlinear Optical Properties of New Schiff's Bases: Experimental Versus Theoretical Study of Inclusion Interactions. *J. Inclusion Phenom. Macrocyclic Chem.* **2013**, *75*, 211−221.
(95) Perry, J. W.; Mansour, K.; Lee, I. Y. S.; Wu, X. L.; Bedworth, P. V.; Chen, C. T.; Ng, D.; Marder, S. R.; Miles, P.; Wada, T.; et al. Organic Optical Limiter with a Strong Nonlinear Absorptive Response. *Science* **1996**, *273*, 1533−1536.
(96) Taki, M.; Wolford, J. L.; O'Halloran, T. V. Emission Ratiometric Imaging of Intracellular Zinc: Design of a Benzoxazole Fluorescent Sensor and its Application in Two-Photon Microscopy. *J. Am. Chem. Soc.* **2004**, *126*, 712−713.
(97) Easwaramoorthi, S.; Jang, S. Y.; Yoon, Z. S.; Lim, J. M.; Lee, C.-W.; Mai, C.-L.; Liu, Y.-C.; Yeh, C.-Y.; Vura-Weis, J.; Wasielewski, M. R.; et al. Structure-Property Relationship for Two-Photon Absorbing Multi-porphyrins: Supramolecular Assembly of Highly-Conjugated Multi-porphyrinic Ladders and Prisms. *J. Phys. Chem. A* **2008**, *112*, 6563−6570.
(98) Ikeda, C.; Yoon, Z. S.; Park, M.; Inoue, H.; Kim, D.; Osuka, A. Helicity Induction and Two-Photon Absorbance Enhancement in Zinc(II) *meso-meso* Linked Porphyrin Oligomers via Intermolecular Hydrogen Bonding Interactions. *J. Am. Chem. Soc.* **2005**, *127*, 534−535.
(99) Hanczyc, P.; Norden, B.; Samoc, M. Two-Photon Absorption of Metal-Organic DNA-probes. *Dalton Trans.* **2012**, *41*, 3123−3125.
(100) Rogers, J. E.; Slagle, J. E.; Krein, D. M.; Burke, A. R.; Hall, B. C.; Fratini, A.; McLean, D. G.; Fleitz, P. A.; Cooper, T. M.; Drobizhev, M.; et al. Platinum Acetylide Two-Photon Chromophores. *Inorg. Chem.* **2007**, *46*, 6483−6494.
(101) Dasari, R. R.; Sartin, M. M.; Cozzuol, M.; Barlow, S.; Perry, J. W.; Marder, S. R. Synthesis and Linear and Nonlinear Absorption Properties of Dendronised Ruthenium(II) Phthalocyanine and Naphthalocyanine. *Chem. Commun.* **2011**, *47*, 4547−4549.
(102) Suponitsky, K. Y.; Masunov, A. E.; Antipin, M. Y. Computational Search for Nonlinear Optical Materials: Are Polarization Functions Important in the Hyperpolarizability Predictions of Molecules and Aggregates? *Mendeleev Commun.* **2009**, *19*, 311−313.
(103) Suponitsky, K. Y.; Masunov, A. E. Supramolecular Step in Design of Nonlinear Optical Materials: Effect of $\pi\cdots\pi$ Stacking Aggregation on Hyperpolarizability. *J. Chem. Phys.* **2013**, *139*, 094310.
(104) Drobizhev, M.; Makarov, N. S.; Hughes, T.; Rebane, A. Resonance Enhancement of Two-Photon Absorption in Fluorescent Proteins. *J. Phys. Chem. B* **2007**, *111*, 14051−14054.